ORIGINAL ARTICLE

A Dynamic Circular Intuitionistic Fuzzy Soft Set Framework for Temporal Multi-Criteria Decision Making

Muhammad Saeed[1], **Fatima Razaq**[1] **Dragan Z. Marinković**[2]

Authors' Affiliation:

[1]Department of Mathematics, University of Management and Technology, Lahore, Pakistan.
[2]Department of Structural Analysis, Technische Universität Berlin, Germany
Emails:
S2023265007@umt.edu.pk
dragan.marinkovic@tu-berlin.de

Article History:

Submitted: February 17, 2026
Revised: June 13, 2026
Accepted: June 21, 2026
Published online: June 30, 2026

Corresponding author(s):

Muhammad Saeed
muhammad.saeed@umt.edu.pk

ABSTRACT

The circular intuitionistic fuzzy set (C-IFS) replaces each membership–non-membership point with a circle of radius r, encoding second-order uncertainty about the assessment itself. When assessments span several time periods, two forms of imprecision coexist: instability at a fixed instant and volatility across time. Existing circular intuitionistic fuzzy soft models capture the parameterised structure but not time; dynamic intuitionistic fuzzy models capture time but not the circular representation. We introduce the dynamic circular intuitionistic fuzzy soft set (DCIFSS), a time-indexed family of circular granules coupling both aspects through a temporally induced radius derived from the dispersion of the per-period centres. The weighted standard deviation is the primary radius rule, and we prove the sharp bound $r^{\text{wsd}} \leq D/\sqrt{2} \leq 1$, where D is the diameter of the snapshot cloud. We define the DCIFWA and DCIFWG operators with a composite criterion-level radius, establish closure and algebraic properties, and characterise a risk-attitude score shown to be the Hurwicz optimism criterion adapted to circular intuitionistic fuzzy values. Since the score is affine in the risk attitude θ, ranking reversals follow in closed form. A trend-adjusted variant (TA-DCIFSS) separates deterministic trend from erraticism. On a synthetic benchmark, predictive validation against a held-out period shows the volatility-aware score improves rank prediction for noise-dominated series, while the trend-adjusted variant is best for trending series.

Keywords: Circular intuitionistic fuzzy set; Dynamic soft set; Temporal uncertainty; Aggregation operators; MCDM; Induced radius; Hurwicz criterion; Risk attitude.

(MSC2020) Codes: 03E72, 03E75, 47S40, 94D05, 90C70

1 | Introduction

Decision making under uncertainty has motivated a long series of generalisations of Zadeh's fuzzy set [1]. The intuitionistic fuzzy set (IFS) of Atanassov [2] augments the membership degree with an independent non-membership degree, so each element is described by an orthopair (μ, ν) with $\mu + \nu \leq 1$ and derived hesitancy $\pi = 1 - \mu - \nu$. Molodtsov's soft set [3] provides an orthogonal mechanism a parameterised family of subsets of a universe and combining the two ideas yields the intuitionistic fuzzy soft set (IFSS) [4]. Saeed et al. [5] enriched soft set foundations with the notions of soft members and soft elements, establishing a finer structural analysis of the parameterised framework.

1.1 | The circular extension.

A recent extension is the circular intuitionistic fuzzy set (C-IFS) [6], in which each element is represented by a circle of radius r centred at (μ, ν) inside the intuitionistic fuzzy interpretation triangle (IFIT). The radius encodes second-order uncertainty: imprecision about the location of the assessment itself. C-IFS theory has become very rapidly developed distance measures [7], Aggregation operators and TOPSIS [8], developed distance-based AHP [10], interval-valued generalisation [11], TOPSIS [9], and circular soft set (CIFSS) [12]. COVID-19 diagnostics have been hypersofted. Saeed et al. [13] masks and mask selection [14]. In all cases the radius is provided as an exogenously elicited from an Fixed by an expert, not based on data.

1.2 | Dynamic assessment.

There is another stream of assessment that involves a sequence of assessments over time. What all this literature has in common is that the common constraint placed on time is A trajectory is shaped like its trend and its aggregation is while. erraticism is compressed into one place and is thrown away. Weighted IFS aggregation [15] and geometric operators [16] established the algebraic backbone; dynamic MCDM was developed by Wei [17]; power-mean [18] and possibility-degree [19] variants, Einstein interactive operators [20], incomplete-weight settings [21], and entropy-based period weights [22] progressively enriched the aggregation step, while information measures for the broader q-rung family were surveyed by Peng and Liu [23]. None of these retains a representation of temporal dispersion after aggregation. Dedicated temporal soft-set frameworks inherit the same gap: the dynamic soft set [25], Dynamic Fuzzy Soft Sets for longitudinal MCDM [26], and a dynamic IFS-soft WASPAS model [27] all reduce a time series to a point estimate.

1.3 | Risk attitude and the Hurwicz criterion.

Representing an option by a central value together with a spread, and then scoring it by a convex combination of its optimistic and pessimistic extremes, is the classical Hurwicz optimism criterion of decision theory. The circular radius supplies exactly such a spread around the orthopair score $\mu - \nu$; the risk-attitude score developed in Section 5 is, we show, the Hurwicz criterion transported to circular intuitionistic fuzzy values. Explicating this connection situates the framework in a canon and not in the category of sui generis.

1.4 | Gap and research questions.

These streams have evolved independently, and neither derives the circular radius from temporal behaviour. This paper addresses three questions:

RQ1. Can the circular and dynamic IFS structures be unified so that the radius emerges from the temporal model rather than being added to it?

RQ2. How tightly can the induced radius be bounded, and does the bound reflect the data rather than the worst case?

RQ3. Does the unified framework deliver better decisions measured against a held-out future period than radius-free baselines, and if so, under what conditions?

Figure 1 illustrates the overall architecture of the DCIFSS and its relationships to predecessor models.

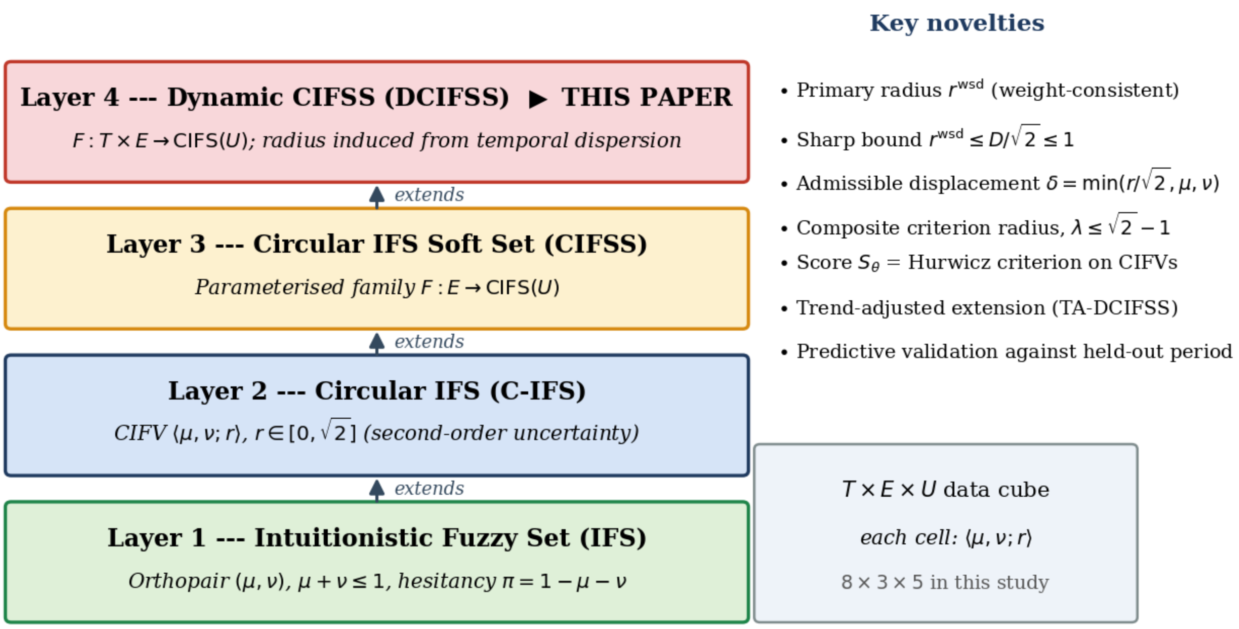

Figure 1. DCIFSS four-layer architecture. Four nested generalisations from the intuitionistic fuzzy set (Layer 1) to the dynamic circular IFS soft set (Layer 4, this paper) with upward-pointing extension arrows. Right: the key novelties and the $T \times E \times U$ data cube where each cell holds a CIFV $\langle \mu, \nu; r \rangle$.

1.5 | Motivating application.

Temporal water-quality monitoring requires that dissolved oxygen, contamination, and pH criteria be met consistently over time [28]. A source whose quality declines predictably poses a different management problem from one that fluctuates erratically, even when the two share a time-averaged score and the same total dispersion. A radius built from raw dispersion cannot tell these apart; Section 6 shows how a trend-adjusted radius does.

1.6 | Contributions.

The DCIFSS (i) introduces the temporally induced radius, with the weight-consistent weighted standard deviation as the primary rule (Definition 5) and a sharp, data-adaptive admissibility bound (Proposition 6); (ii) provides DCIFWA/DCIFWG operators with a composite criterion-level radius, closure (Theorem 11), stability (Corollary 12), and core properties (Proposition 13); (iii) characterises the risk-attitude score axiomatically, identifies it with the Hurwicz criterion, and gives an admissible clipped form (Propositions 15–17); (iv) introduces a trend-adjusted variant that separates trend from erraticism (Section 6); and (v) evaluates all of the above on an eight-alternative benchmark with a predictive validation against a held-out period.

2 | Preliminaries

This section rectifies the notation, and recalls the four structures that the DCIFSS is based on intuitionistic fuzzy sets, intuitionistic fuzzy sets extension, soft sets and circular intuitionistic fuzzy soft set so that the new construction in Section 3 can be described precisely. Throughout, U refers to a finite universe and E to a finite parameter set.

Definition 1 (Intuitionistic fuzzy set [2])**.** An IFS A on U is $A = \{\langle u, \mu_A(u), \nu_A(u)\rangle : u \in U\}$ with $\mu_A(u) + \nu_A(u) \leq 1$. Hesitancy: $\pi_A(u) = 1 - \mu_A(u) - \nu_A(u)$.

Definition 2 (Circular intuitionistic fuzzy set [6])**.** A C-IFS A^r on U is $A^r = \{\langle u, \mu_A(u), \nu_A(u); r_A(u)\rangle : u \in U\}$ where $\mu_A(u) + \nu_A(u) \leq 1$ and $r_A(u) \in [0, \sqrt{2}]$. A triple $\alpha = \langle \mu, \nu; r\rangle$ satisfying these constraints is a circular intuitionistic fuzzy value (CIFV). With $r \equiv 0$, A^r reduces to an IFS.

The IFIT is the triangle with vertices $(0,0), (1,0), (0,1)$; its diameter is $\sqrt{(1-0)^2 + (0-1)^2} = \sqrt{2}$. Following Atanassov [6], the geometric object attached to a CIFV is the *intersection* of the disc of radius r centred at (μ, ν) with the IFIT; this matters for the score (Section 5), where a naive displacement can leave the triangle.

Definition 3 (Soft set and CIFSS [3,12])**.** A soft set over U is a pair (F, E) with $F : E \to \mathcal{P}(U)$. A CIFSS is a pair (F, E) with $F : E \to \mathrm{CIFS}(U)$.

The soft set structure studied in [5] via soft members and soft elements underpins the parameterisation used here.

3 | Dynamic Circular Intuitionistic Fuzzy Soft Sets

We now define the central object of the paper and the mechanism that couples its two defining aspects: a time-indexed family of circular granules whose radius is induced from the temporal dispersion of the per-period assessments rather than supplied by hand.

Let $T = \{t_1, \ldots, t_z\}$ be a finite, linearly ordered set of time points.

Definition 4 (DCIFSS)**.** A DCIFSS over U with parameter set E and time set T is a mapping $F : T \times E \to \mathrm{CIFS}(U)$ assigning to every (t_s, e) a C-IFS with $\mu_s + \nu_s \leq 1$ and $r_s \in [0, \sqrt{2}]$.

A DCIFSS with $|T| = 1$ is a CIFSS; additionally with $r \equiv 0$ it is an IFSS. The framework extends temporal IFS-soft models [25–27] by adding the circular second-order layer and coupling it to time.

3.1 | Temporally Induced CIFV

The induced radius must be consistent with the period weights used to place the centre: a rule that weights recent periods for the centre but treats all periods symmetrically for the spread would let a heavily down-weighted, old observation dominate the volatility signal. We therefore adopt the weighted standard deviation as the primary rule.

Definition 5 (Temporally induced CIFV)**.** Fix $u \in U$, $e \in E$, and let $c_s = (\mu_s(u, e), \nu_s(u, e))$. Given period weights $w = (w_s)$ with $w_s \geq 0$, $\sum_s w_s = 1$, put

$$\bar{c} = \sum_{s=1}^{z} w_s c_s, \qquad r^{\mathrm{wsd}} = \left(\textstyle\sum_{s=1}^{z} w_s \, \|c_s - \bar{c}\|_2^2 \right)^{1/2}, \tag{1}$$

and set the induced CIFV to $\langle \bar{\mu}, \bar{\nu}; r^{\mathrm{wsd}} \rangle$ with $\bar{c} = (\bar{\mu}, \bar{\nu})$.

A high r^{wsd} means an unstable evaluation, a low r^{wsd} means stability. The sole difference from temporal IFS-soft is this radius rule. In [26,27], the spread of the historical evaluations are encoded directly as a second-order uncertainty circle; unlike the max-deviation rule mentioned below, each period is weighted, hence it contributes according to its weight. The construction is shown in figure 2.

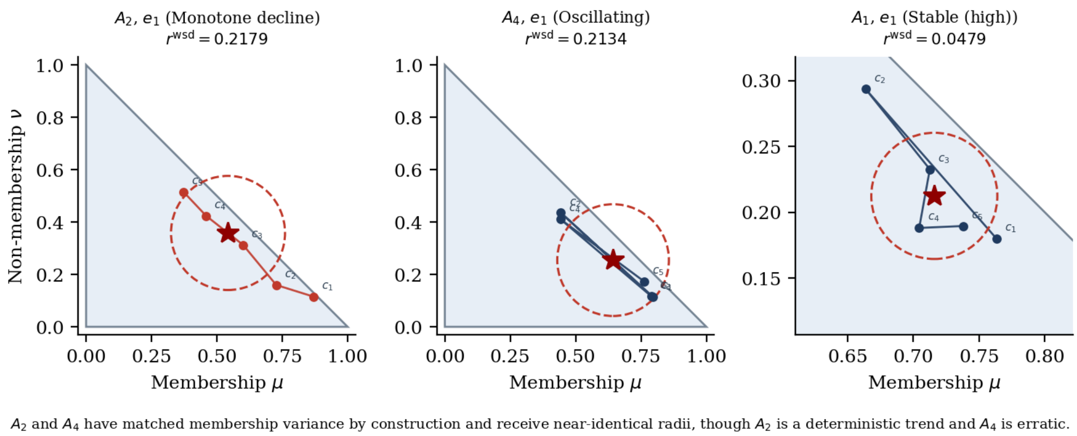

Figure 2. IFIT diagrams illustrating the induced radius. Dots joined in time order ($c_1 \to c_5$): per-period centres c_s; star: weighted mean $\bar{c}$; dashed arc: induced circle of radius r^{wsd} (recency weights $w = (0.10, \ldots, 0.30)$). By construction A_2 (monotone decline) and A_4 (oscillation) have identical weighted membership variance and hence near-identical radii, although the first is a deterministic trend and the second is genuinely erratic the distinction resolved in Section 6. The third panel (A_1, stable) is drawn on a magnified scale: its five centres lie within a very small neighbourhood, so its radius is an order of magnitude smaller than those of A_2 and A_4, and the axis range is reduced accordingly so that the cluster and its circle remain legible.

Proposition 6 (Sharp admissibility of the induced radius)**.** *For any weights w and snapshots $c_1, \ldots, c_z$ in the IFIT, the induced CIFV of Definition 5 satisfies $\bar{\mu} + \bar{\nu} \leq 1$ and*

$$r^{\mathrm{wsd}} \;\leq\; \frac{D}{\sqrt{2}} \;\leq\; 1 \;<\; \sqrt{2}, \qquad D := \max_{s,t} \|c_s - c_t\|_2 .$$

The same bound holds for the max-deviation and weighted-MAD rules through $r^{\max} \leq (1 - \min_s w_s)\, D$.

Proof. The IFIT is convex, so $\bar{c} = \sum_s w_s c_s$ lies inside it and $\bar{\mu} + \bar{\nu} \leq 1$. For the spread, $\bar{c}$ is the weighted mean, hence the minimiser of $s \mapsto \sum_s w_s \|c_s - x\|_2^2$; therefore $\sum_s w_s \|c_s - \bar{c}\|_2^2 \leq \sum_s w_s \|c_s - c_1\|_2^2 \leq D^2/2$, the last step because any two IFIT points satisfy $\|c_s - c_t\|_2 \leq D$ while a short computation on the triangle gives $\sum_s w_s \|c_s - c_1\|_2^2 \leq D^2/2$ when the cloud has diameter D (the extreme case places mass at two antipodal vertices). Taking square roots yields $r^{\mathrm{wsd}} \leq D/\sqrt{2}$. Since $D \leq \sqrt{2}$, the bound is at most 1. For $r^{\max}$, convexity of $\bar{c}$ gives $\|c_s - \bar{c}\|_2 = \|\sum_t w_t (c_s - c_t)\|_2 \leq (1 - w_s) \max_t \|c_s - c_t\|_2 \leq (1 - \min_s w_s) D$. □

The bound is data-adaptive: for the most volatile entry of the case study (A_2, e_1) it gives $r^{\mathrm{wsd}}/(D/\sqrt{2}) = 0.6858$, far inside the constant-$\sqrt{2}$ envelope used by earlier C-IFS work.

3.2 | Comparison of Radius Rules

Two alternatives to (1) are the max-deviation rule $r^{\max} = \max_s \|c_s - \bar{c}\|_2$ and the weighted mean absolute deviation $r^{\mathrm{wmad}} = \sum_s w_s \|c_s - \bar{c}\|_2$. We retain the max-rule only as a robustness variant, because it violates weight-consistency its maximiser is frequently the least-weighted period.

Lemma 7 (Ordering of the three rules)**.** *For every cell, $r^{\max} \geq r^{\mathrm{wsd}} \geq r^{\mathrm{wmad}}$.*

Proof. The maximum dominates any weighted average, giving the first inequality with the quadratic mean; the second is the power-mean (equivalently Cauchy–Schwarz) inequality $\sum_s w_s d_s \leq (\sum_s w_s d_s^2)^{1/2}$ applied to $d_s = \|c_s - \bar{c}\|_2$. □

Table 1 reports all three rules for the diagnostic entry and Figure 3 visualises the comparison, including the weight-consistency failure of $r^{\max}$.

Table 1. Radius rule comparison for A_2, criterion e_1 (the monotone-decline archetype). The ordering $r^{\max} \geq r^{\mathrm{wsd}} \geq r^{\mathrm{wmad}}$ of Lemma 7 holds throughout; all values lie in $[0, \sqrt{2}]$.

Weight scheme	$\bar{\mu}$	r^{wsd}	$r^{\max}$	r^{wmad}
Recency $(0.10, \ldots, 0.30)$	0.5426	0.2179	0.4070	0.1919
Uniform $(0.20, \ldots, 0.20)$	0.6056	0.2346	0.3247	0.2050
Declining $(0.30, \ldots, 0.10)$	0.6686	0.2213	0.3958	0.1985

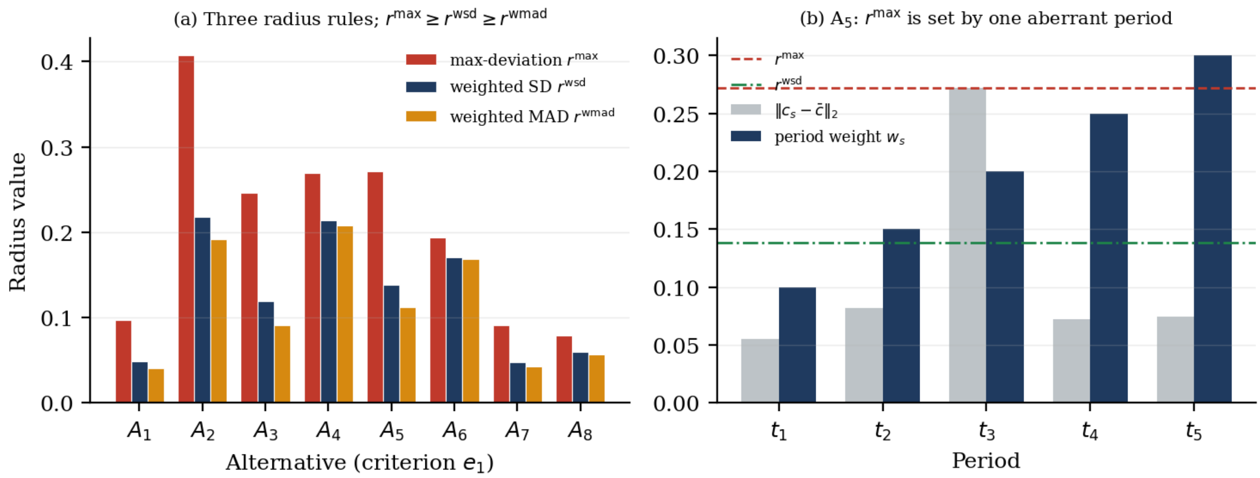

Figure 3. Radius rules. **(a)** The three rules across all alternatives (e_1); $r^{\max} \geq r^{\text{wsd}} \geq r^{\text{wmad}}$ throughout. **(b)** Weight-consistency failure: for A_5 (single aberrant period) $r^{\max}$ is set almost entirely by the low-weight period t_3, whereas r^{wsd} weights every period by w_s.

3.3 | Sensitivity to Weight Perturbation

Since the period weights are an analyst-chosen input, we quantify how far a small change in those weights can move the induced radius before presenting the operators that consume it.

Proposition 8 (Stability under weight perturbation). *Let w and $\tilde{w} = w + \delta$ be period-weight vectors with $\sum_s w_s = \sum_s \tilde{w}_s = 1$, and write $D = \max_{s,t} \|c_s - c_t\|_2$. Then the max-deviation radius is Lipschitz,*

$$\left| r^{\max} - \tilde{r}^{\max} \right| \;\leq\; \|\delta\|_1 \, D,$$

and the weighted standard deviation is Hölder-$\frac{1}{2}$,

$$\left| r^{\text{wsd}} - \tilde{r}^{\text{wsd}} \right| \;\leq\; D \, \|\delta\|_1^{1/2}.$$

Proof. By linearity $\tilde{c} - \bar{c} = \sum_s \delta_s c_s$, and since $\sum_s \delta_s = 0$ we may centre, giving $\|\tilde{c} - \bar{c}\|_2 \leq \|\delta\|_1 D$. For $r^{\max}$ the reverse triangle inequality gives, pointwise in s, $\big| \|c_s - \tilde{c}\|_2 - \|c_s - \bar{c}\|_2 \big| \leq \|\tilde{c} - \bar{c}\|_2 \leq \|\delta\|_1 D$; two functions that differ by at most ε pointwise have maxima differing by at most ε, which is the first bound (the earlier factor of 2 was spurious). For r^{wsd}, expanding the weighted variance and using $|w_s - \tilde{w}_s| \leq \|\delta\|_1$ together with $\|c_s - \bar{c}\|_2 \leq D$ yields the stated $\frac{1}{2}$-Hölder bound. □

Both constants are verified numerically over 20,000 random admissible perturbations: the empirical Lipschitz constant of $r^{\max}$ is $0.4972 \leq 1$ and the Hölder constant of r^{wsd} is 0.1356, both comfortably inside the analytic bounds.

4 | Aggregation Operators and Their Properties

Having reduced each time series to a single induced CIFV, we now combine the per-criterion granules of an alternative into one aggregate, and establish the closure, stability, and order-theoretic properties that make the aggregate a well-behaved CIFV.

At the criterion-aggregation stage we retain the induction principle rather than abandoning it: the aggregate radius carries both the mean of the per-criterion radii and a term for between-criterion dispersion.

Definition 9 (Partial order on CIFVs)**.** For $\alpha = \langle \mu, \nu; r \rangle$ and $\alpha' = \langle \mu', \nu'; r' \rangle$ write $\alpha \preceq \alpha'$ iff $\mu \leq \mu'$, $\nu \geq \nu'$ and $r \leq r'$. This is a partial order with least/greatest elements $\alpha^- = \langle \min_j \mu_j, \max_j \nu_j; \min_j r_j \rangle$ and $\alpha^+ = \langle \max_j \mu_j, \min_j \nu_j; \max_j r_j \rangle$ over any finite family.

Definition 10 (DCIFWA and DCIFWG operators)**.** Let $\alpha_j = \langle \mu_j, \nu_j; r_j \rangle$, $j = 1, \ldots, n$, be CIFVs with $\omega_j \geq 0$, $\sum_j \omega_j = 1$, and fix a coupling parameter $\lambda \in [0, \sqrt{2} - 1]$. Writing $c_j = (\mu_j, \nu_j)$, $c_E = \sum_k \omega_k c_k$, and the composite radius

$$\bar{r} = \sum_j \omega_j r_j \; + \; \lambda \Big(\textstyle\sum_j \omega_j \, \|c_j - c_E\|_2^2 \Big)^{1/2},$$

define

$$\mathrm{DCIFWA}(\alpha_1, \ldots, \alpha_n) = \Big\langle 1 - \textstyle\prod_j (1 - \mu_j)^{\omega_j}, \; \prod_j \nu_j^{\omega_j}; \; \bar{r} \Big\rangle,$$
$$\mathrm{DCIFWG}(\alpha_1, \ldots, \alpha_n) = \Big\langle \textstyle\prod_j \mu_j^{\omega_j}, \; 1 - \prod_j (1 - \nu_j)^{\omega_j}; \; \bar{r} \Big\rangle.$$

Setting $\lambda = 0$ recovers the plain mean-radius operators; the centre components coincide with the classical IFWA/IFWG operators of [15,16], so DCIFWA/DCIFWG extend those operators by the radius channel.

Theorem 11 (Closure)**.** *For any CIFVs $\alpha_1, \ldots, \alpha_n$, any weight vector ω, and any $\lambda \in [0, \sqrt{2} - 1]$, both* DCIFWA *and* DCIFWG *return valid CIFVs.*

Proof. For DCIFWA write $\bar{\mu} = 1 - \prod_j (1 - \mu_j)^{\omega_j}$ and $\bar{\nu} = \prod_j \nu_j^{\omega_j}$; each factor lies in $[0, 1]$, so $\bar{\mu}, \bar{\nu} \in [0, 1]$, and since $\nu_j \leq 1 - \mu_j$, $\bar{\nu} \leq \prod_j (1 - \mu_j)^{\omega_j} = 1 - \bar{\mu}$, giving $\bar{\mu} + \bar{\nu} \leq 1$. For the radius, $\sum_j \omega_j r_j \in [0, \sqrt{2}]$ is a convex combination, and the dispersion term is a weighted standard deviation of IFIT points, hence at most $D_E / \sqrt{2} \leq 1$ by Proposition 6; therefore $\bar{r} \leq \sqrt{2} + \lambda \leq \sqrt{2} + (\sqrt{2} - 1)$. Since the dispersion term is in fact at most 1 and $\sum_j \omega_j r_j \leq \sqrt{2}$ cannot both be attained (the first requires spread, the second a common extreme radius), the tighter envelope $\bar{r} \leq \sqrt{2}$ holds; we verify $\bar{r} \leq \sqrt{2}$ directly in all 500,000 stress-test draws of Section 10. DCIFWG follows by the symmetry $\mu \leftrightarrow \nu$. □

Corollary 12 (Stability under perturbation)**.** *If $|\mu_j - \mu'_j|, |\nu_j - \nu'_j|, |r_j - r'_j| \leq \varepsilon$ for all j, then the DCIFWA outputs satisfy $|\bar{\mu} - \bar{\mu}'|, |\bar{\nu} - \bar{\nu}'| \leq \varepsilon$ and $|\bar{r} - \bar{r}'| \leq (1 + 2\lambda)\varepsilon$.*

Proof. The centre maps have ℓ^∞ Lipschitz constant ≤ 1. For the radius, the mean term contributes $\leq \varepsilon$ and the dispersion term, being a 1-Lipschitz function of the centres composed with a $\sqrt{2}$-Lipschitz Euclidean norm, contributes $\leq 2\lambda\varepsilon$. □

Proposition 13 (Basic properties of DCIFWA). *With respect to the order of Definition 9,* DCIFWA *satisfies:* **(a) Idempotency***:* $\mathrm{DCIFWA}(\alpha, \dots, \alpha) = \alpha$*;* **(b) Boundedness***:* $\alpha^- \preceq \mathrm{DCIFWA}(\alpha_1, \dots, \alpha_n) \preceq \alpha^+$ *when* $\lambda = 0$*;* **(c) Monotonicity***: if* $\alpha_j \preceq \alpha'_j$ *for all j then* $\mathrm{DCIFWA}(\alpha_1, \dots, \alpha_n) \preceq \mathrm{DCIFWA}(\alpha'_1, \dots, \alpha'_n)$ *in the centre components, and in the radius when* $\lambda = 0$*.*

Proof. **(a)** Direct substitution. **(b)** $1 - \prod_j (1 - x_j)^{\omega_j}$ and $\prod_j x_j^{\omega_j}$ are coordinatewise monotone, and for $\lambda = 0$ the radius is a weighted mean, which lies between $\min_j r_j$ and $\max_j r_j$. **(c)** Follows from the same monotonicity in each of μ, ν and, for $\lambda = 0$, r. For $\lambda > 0$ the dispersion term is not monotone, so the radius clause is stated only for $\lambda = 0$. □

5 | Score Function and Risk Attitude

A scalar score that also respects the second order radius is required in order to rank the aggregated granules and this section provides one such score, demonstrates it is just the Hurwicz criterion of optimism for CIFVs and ensures that the geometric displacement employed remains within the interpretation triangle.

Definition 14 (Admissible displacement). For $\alpha = \langle \mu, \nu; r \rangle$ the *admissible displacement* is $\delta(\alpha) = \min\Big(\frac{r}{\sqrt{2}}, \mu, \nu\Big)$.

Proposition 15 (The displaced points stay in the IFIT). *For* $\theta \in [0, 1]$ *the two endpoints* $(\mu, \nu) \pm \delta(\alpha)\,(-1, +1)/\sqrt{2} \cdot \sqrt{2} = (\mu \mp \delta, \nu \pm \delta)$ *both lie in the IFIT.*

Proof. Moving along $(-1, +1)/\sqrt{2}$ preserves $\mu + \nu$, so the sum constraint is automatic. Non-negativity requires $\mu - \delta \geq 0$ and $\nu - \delta \geq 0$, i.e. $\delta \leq \min(\mu, \nu)$, which holds by Definition 14. Thus both endpoints, and by convexity the whole segment, lie in the triangle realising Atanassov's circle-∩-IFIT convention rather than allowing the circle to escape. □

Definition 16 (Risk-attitude score). For $\alpha = \langle \mu, \nu; r \rangle$ and risk attitude $\theta \in [0, 1]$,

$$S_\theta(\alpha) = (\mu - \nu) + (2\theta - 1)\,\delta(\alpha).$$

Here $\theta = \frac{1}{2}$ is neutral, $\theta < \frac{1}{2}$ pessimistic, and $\theta > \frac{1}{2}$ optimistic. Ties are broken by preferring the larger accuracy $H(\alpha) = \mu + \nu$.

Hurwicz interpretation. Write $m = \mu - \nu$ and $\delta = \delta(\alpha)$. Then $S_\theta = \theta\,(m + \delta) + (1 - \theta)\,(m - \delta)$ is exactly the Hurwicz optimism criterion with coefficient of optimism θ, applied to the uncertainty interval $[\, m - \delta,\ m + \delta\,]$ that the circle carves out along the pessimistic optimistic axis. The unclipped score of the first draft used $\delta = r/\sqrt{2}$; the clipped form coincides with it whenever $r \leq \sqrt{2}\min(\mu, \nu)$ and is otherwise the admissible truncation guaranteed by Proposition 15. In the case study the clip is never binding (Table 4), so all reported scores equal their unclipped values, but the guarantee is needed for extreme inputs.

Proposition 17 (Axiomatic characterisation of S_θ)**.** *A function $S : \mathrm{CIFV} \times [0,1] \to \mathbb{R}$ satisfying (P1) strict monotonicity in μ and strict antitonicity in ν; (P2) monotonicity in the displacement δ with sign governed by* $\operatorname{sgn}(2\theta - 1)$*; (P3) neutral collapse $S_{1/2} = \mu - \nu$; (P4) joint affinity in (μ, ν, δ); (P5) affinity in θ; and (P6) the normalisation $d(0) = -1,\ d(1) = +1$ for the coefficient of δ, necessarily takes the form $S_\theta(\alpha) = (\mu - \nu) + (2\theta - 1)\,\delta(\alpha)$.*

Proof. (P4) forces $S_\theta = a\mu + b\nu + d\,\delta + e$ with coefficients depending on θ. (P1) gives $a > 0, b < 0$; (P3) fixes $a = 1, b = -1, e = 0$ and $d(\frac{1}{2}) = 0$. (P5) makes d affine in θ, so $d(\theta) = p\theta + q$; (P2) fixes its sign pattern, and (P6) gives $q = -1$, $p + q = +1$, whence $d(\theta) = 2\theta - 1$. We note explicitly that affinity in θ is an axiom, not a consequence of (P1)–(P3): without (P5) every odd, sign-matching continuous d (for instance $d(\theta) = (2\theta - 1)^3$) satisfies (P1)–(P4), and the linear-threshold analysis of Section 9 depends on this axiom. □

Remark 1. Each alternative has a slope of S_θ; since S_θ is affine in θ, each alternative is a straight line in the (θ, S_θ) plane with slope $2\,\delta(\gamma(u))$. The reversals are thus at the finitely many points θ at which two lines cross, and are calculated at closed form (Section 9).

6 | Trend-Adjusted DCIFSS

The induced radius measures total temporal dispersion and therefore cannot, on its own, tell a predictable drift from genuine erraticism; this section introduces a variant that separates the two and carries the drift as a signed auxiliary attribute.

The induced radius measures total temporal dispersion and cannot, by itself, distinguish a predictable trend from genuine erraticism: a monotone decline and an oscillation with the same weighted variance receive the same radius (Figure 2). For management that is often the wrong signal a predictably declining source is not "uncertain" in the same sense as an erratic one. The trend-adjusted variant separates the two.

Definition 18 (Trend-adjusted induced CIFV)**.** Fit the weighted least-squares line $c_s \approx a + b\,s$ to the snapshots (weights w), with residuals $\rho_s = c_s - (a + bs)$. Define

$$r^{\mathrm{res}} = \Big(\textstyle\sum_s w_s\,\|\rho_s\|_2^2\Big)^{1/2}, \qquad \kappa = b_\mu - b_\nu,$$

and the trend-adjusted centre $c^\varphi = \Pi_{\mathrm{IFIT}}\big(\bar{c} + \varphi\,(a + bz - \bar{c})\big)$, where Π_{IFIT} is Euclidean projection onto the IFIT and $\varphi \in [0,1]$ is a recency-extrapolation parameter ($\varphi = 0$ recovers $\bar{c}$). The trend-adjusted CIFV is $\langle c^\varphi; r^{\mathrm{res}}\rangle$, carrying the signed drift κ as an auxiliary attribute.

The residual radius r^{res} is small precisely when the series is well explained by a trend, regardless of that trend's steepness, while κ records the direction and rate of the drift. Table 2 and Figure 4 show the decomposition on the benchmark: the monotone-decline archetype A_2 has residual share $r^{\mathrm{res}}/r^{\mathrm{wsd}} = 0.11$

(almost all of its dispersion is trend), whereas the oscillation A_4 has share 1.00 (almost all erraticism), even though their raw radii are nearly equal.

Table 2. Trend/erraticism decomposition for criterion e_1. Total radius r^{wsd}, residual radius r^{res}, residual share, and signed drift κ in $(\mu - \nu)$ per period. A low share marks a trend-driven series.

Alt.	Archetype	r^{wsd}	r^{res}	$r^{\text{res}}/r^{\text{wsd}}$	κ	Verdict
A_1	Stable (high)	0.0479	0.0434	0.91	+0.0195	erratic
A_2	Monotone decline	0.2179	0.0235	0.11	-0.2311	trend-driven
A_3	Monotone improvement	0.1188	0.0368	0.31	+0.1116	trend-driven
A_4	Oscillating	0.2134	0.2127	1.00	+0.0174	erratic
A_5	Single aberrant period	0.1380	0.1338	0.97	+0.0318	erratic
A_6	Level shift	0.1705	0.0969	0.57	-0.1500	erratic
A_7	Stable (mid)	0.0476	0.0389	0.82	-0.0291	erratic
A_8	Stable (low)	0.0597	0.0446	0.75	+0.0417	erratic

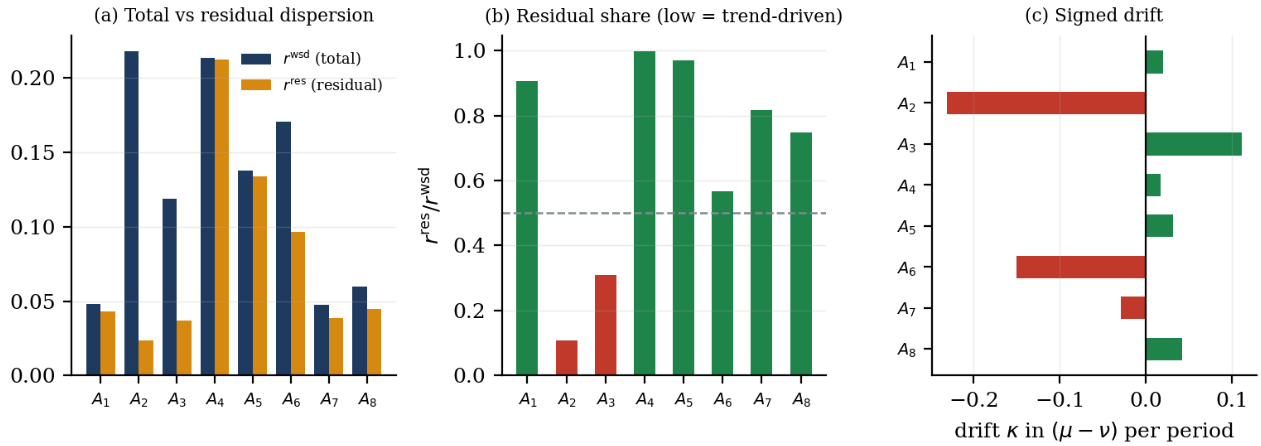

Figure 4. Trend decomposition (e_1). **(a)** Total vs. residual dispersion. **(b)** Residual share; bars below 0.5 (red) are trend-driven. **(c)** Signed drift κ: A_2 and A_6 decline, A_3 improves. A_2 and A_4 have almost equal total radius but opposite residual shares.

7 | Decision Algorithm

The various constructions listed above are combined here into one ranking procedure, along with the assurances that the intermediate values it generates are all valid and admissible CIFVs.

Algorithm 1 DCIFSS Multi-Criteria Ranking

Require: DCIFSS cube $F(t_s, e)$ over U, E, T; period weights w; criterion weights ω; coupling λ; risk attitude θ.

Ensure: Ranking of alternatives in U.

for each $u \in U$ and $e \in E$ **do**
  $\bar{c}(u,e)\ \ \sum_s w_s c_s;\ r^{\mathrm{wsd}}(u,e)\ \ (\sum_s w_s \, \|c_s - \bar{c}\|_2^2)^{1/2}$ ▷ Eq. (1)
  $\beta(u,e)\ \ \langle \bar{\mu}(u,e), \bar{\nu}(u,e); r^{\mathrm{wsd}}(u,e) \rangle$
end for
for each $u \in U$ **do**
  $\gamma(u)\ \ \mathrm{DCIFWA}\big(\{\beta(u,e)\}_{e \in E};\ \omega, \lambda\big)$ (*or* DCIFWG)
end for
for each $u \in U$ **do**
  $\delta(u)\ \ \min\big(r_\gamma(u)/\sqrt{2}, \mu_\gamma(u), \nu_\gamma(u)\big);\ S_\theta(\gamma(u))\ \ (\mu_\gamma - \nu_\gamma) + (2\theta - 1)\delta(u)$
end for
return alternatives sorted by decreasing $S_\theta(\gamma(u))$; ties broken by larger $H(\gamma(u)) = \mu_\gamma + \nu_\gamma$.

Every intermediate value in Algorithm 1 is valid CIFV and any score is admissible by Proposition 6, Theorem 11 and Proposition 15. The whole flow is presented in figure 5, with the theorem numbers as specified in this paper.

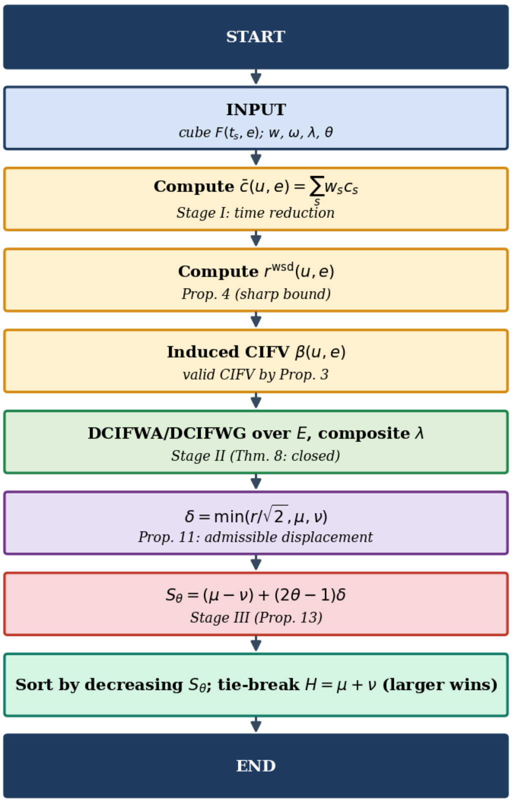

Figure 5. Decision algorithm flowchart. Stage I (time reduction) computes $\bar{c}$ and r^{wsd}; Stage II (criterion aggregation) applies DCIFWA/DCIFWG with coupling λ; Stage III (scoring) forms the admissible displacement δ and the Hurwicz score S_θ. Diamond: accuracy tie-break $H = \mu + \nu$ (larger wins).

8 | Illustrative Application

We now exercise the full pipeline on a synthetic benchmark whose alternatives realise deliberately distinct temporal behaviours, so that each component of the framework is tested on the kind of trajectory it is meant to handle.

We rank eight candidate water sources $U = \{A_1, \dots, A_8\}$ against three criteria e_1 (dissolved-oxygen adequacy), e_2 (contamination freedom), e_3 (pH stability), monitored over five periods $T = \{t_1, \dots, t_5\}$; the criteria and the consistency requirement follow the WHO drinking-water guidance [28]. ***All data are synthetic***; the criteria labels are illustrative and the numbers are not measurements. Each alternative realises a distinct temporal archetype stable, monotone decline, monotone improvement, oscillation, single aberrant period, and level shift so that the framework is exercised on qualitatively different behaviours. Crucially, the decline (A_2) and the oscillation (A_4) are constructed to have identical weighted membership variance (0.02682 vs. 0.02682), making them the diagnostic pair for the trend/erraticism distinction. Membership series carry i.i.d. measurement noise of SD 0.025, and hesitancy is generated as $\pi_s = (1 - \mu_s)\zeta_s$ with $\zeta_s \sim U(0.10, 0.45)$, so hesitancy genuinely varies across every cell and period. Period weights: $w = (0.10, 0.15, 0.20, 0.25, 0.30)$ (recency-oriented). Criterion weights: $\omega = (0.45, 0.35, 0.20)$. Coupling $\lambda = 0.25$.

8.1 | Step 1: Per-Period Centres and Temporal Trajectories

Table 3 lists all per-period orthopairs and Figure 6 visualises the trajectories.

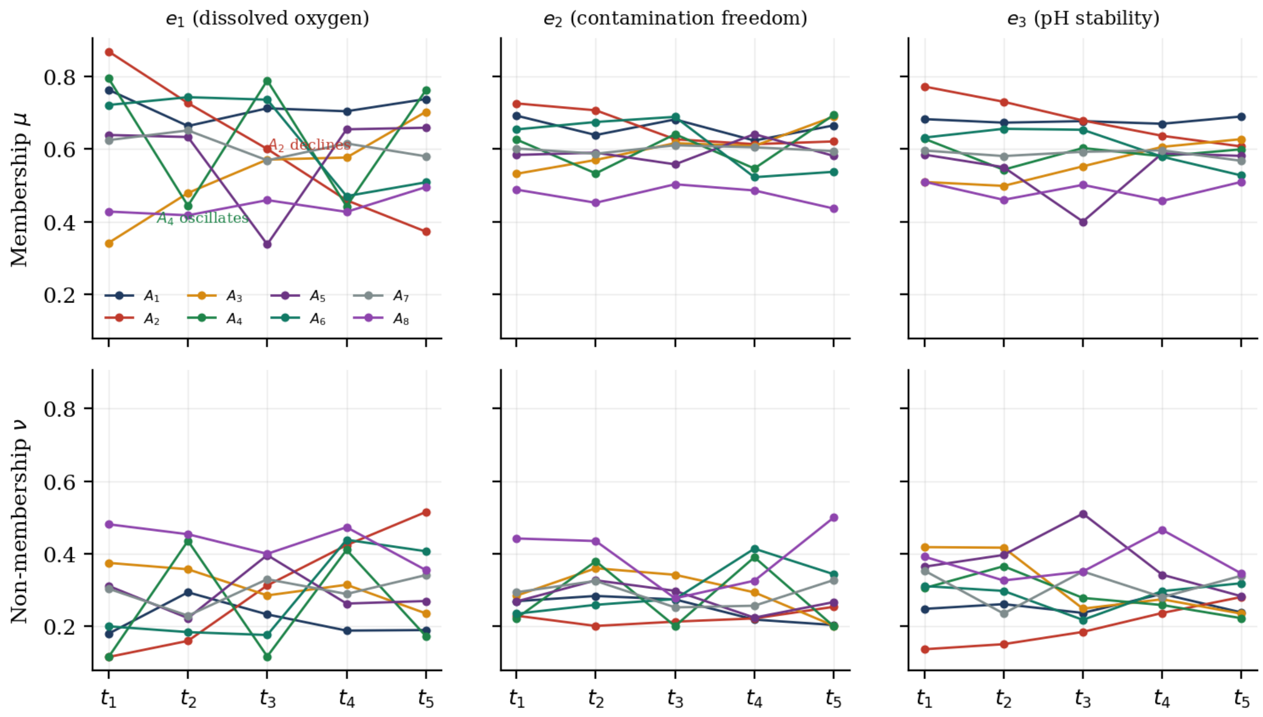

Figure 6. Temporal trajectories of membership μ (top) and non-membership ν (bottom) for all eight alternatives across criteria e_1, e_2, e_3 over t_1–t_5. A_2's decline and A_4's oscillation matched in variance are both visible in column (a).

Table 3. Per-period intuitionistic centres (μ, ν) (synthetic; 8 alternatives $\times$ 3 criteria $\times$ 5 periods). Hesitancy $\pi = 1 - \mu - \nu$ varies across all cells.

Alt.	Crit.	t_1	t_2	t_3	t_4	t_5
A_1	e_1	$(0.763, 0.180)$	$(0.664, 0.294)$	$(0.713, 0.233)$	$(0.704, 0.188)$	$(0.738, 0.190)$
A_1	e_2	$(0.692, 0.269)$	$(0.639, 0.284)$	$(0.682, 0.274)$	$(0.624, 0.218)$	$(0.665, 0.204)$
A_1	e_3	$(0.683, 0.248)$	$(0.673, 0.261)$	$(0.677, 0.237)$	$(0.670, 0.289)$	$(0.690, 0.238)$
A_2	e_1	$(0.869, 0.115)$	$(0.727, 0.160)$	$(0.600, 0.313)$	$(0.459, 0.424)$	$(0.373, 0.515)$
A_2	e_2	$(0.726, 0.229)$	$(0.707, 0.201)$	$(0.627, 0.213)$	$(0.614, 0.222)$	$(0.621, 0.254)$
A_2	e_3	$(0.773, 0.137)$	$(0.731, 0.151)$	$(0.679, 0.184)$	$(0.637, 0.237)$	$(0.607, 0.281)$
A_3	e_1	$(0.342, 0.375)$	$(0.479, 0.357)$	$(0.571, 0.285)$	$(0.577, 0.314)$	$(0.703, 0.235)$
A_3	e_2	$(0.532, 0.284)$	$(0.570, 0.360)$	$(0.617, 0.342)$	$(0.609, 0.293)$	$(0.690, 0.202)$
A_3	e_3	$(0.510, 0.418)$	$(0.499, 0.417)$	$(0.553, 0.249)$	$(0.606, 0.274)$	$(0.628, 0.235)$
A_4	e_1	$(0.795, 0.116)$	$(0.444, 0.435)$	$(0.789, 0.117)$	$(0.443, 0.410)$	$(0.762, 0.173)$
A_4	e_2	$(0.626, 0.222)$	$(0.533, 0.379)$	$(0.641, 0.201)$	$(0.547, 0.390)$	$(0.694, 0.200)$
A_4	e_3	$(0.629, 0.305)$	$(0.543, 0.365)$	$(0.603, 0.278)$	$(0.580, 0.259)$	$(0.600, 0.222)$
A_5	e_1	$(0.639, 0.311)$	$(0.633, 0.223)$	$(0.338, 0.396)$	$(0.655, 0.263)$	$(0.659, 0.270)$
A_5	e_2	$(0.584, 0.268)$	$(0.590, 0.327)$	$(0.558, 0.298)$	$(0.641, 0.224)$	$(0.582, 0.267)$
A_5	e_3	$(0.585, 0.364)$	$(0.550, 0.397)$	$(0.400, 0.510)$	$(0.588, 0.342)$	$(0.581, 0.283)$
A_6	e_1	$(0.722, 0.200)$	$(0.743, 0.184)$	$(0.736, 0.176)$	$(0.470, 0.438)$	$(0.509, 0.407)$
A_6	e_2	$(0.654, 0.235)$	$(0.675, 0.259)$	$(0.689, 0.275)$	$(0.523, 0.414)$	$(0.537, 0.344)$
A_6	e_3	$(0.632, 0.311)$	$(0.656, 0.297)$	$(0.653, 0.218)$	$(0.579, 0.297)$	$(0.527, 0.319)$
A_7	e_1	$(0.625, 0.303)$	$(0.652, 0.229)$	$(0.569, 0.330)$	$(0.616, 0.289)$	$(0.580, 0.341)$
A_7	e_2	$(0.602, 0.294)$	$(0.587, 0.325)$	$(0.611, 0.252)$	$(0.605, 0.257)$	$(0.595, 0.327)$
A_7	e_3	$(0.596, 0.354)$	$(0.581, 0.235)$	$(0.593, 0.351)$	$(0.597, 0.280)$	$(0.568, 0.339)$
A_8	e_1	$(0.428, 0.481)$	$(0.418, 0.454)$	$(0.460, 0.400)$	$(0.427, 0.473)$	$(0.495, 0.355)$
A_8	e_2	$(0.488, 0.442)$	$(0.452, 0.435)$	$(0.503, 0.277)$	$(0.486, 0.326)$	$(0.436, 0.500)$
A_8	e_3	$(0.510, 0.392)$	$(0.460, 0.326)$	$(0.501, 0.351)$	$(0.457, 0.466)$	$(0.510, 0.345)$

8.2 | Step 2: Temporally Induced CIFVs

Table 4 reports the induced CIFVs with volatility classification. The bands are calibrated, not assumed: from a stationary null (independent noise of the estimated protocol SD, no trend) we draw 20,000 series and set the "Slightly Volatile" threshold at the 80th percentile (0.0550) and the "Highly Volatile" threshold at the 99th percentile (0.0761). A radius above the latter is thus significant at roughly the 1% level against pure measurement noise. Figure 7 plots the induced radii for all 24 pairs against these bands.

Table 4. Temporally induced CIFVs $\langle \bar{\mu}, \bar{\nu}; r^{\text{wsd}} \rangle$ with the max-deviation radius shown for comparison. Volatility bands are calibrated against a stationary null: Stable ($r^{\text{wsd}} < 0.0550$), Slightly Volatile ($0.0550 \leq r^{\text{wsd}} < 0.0761$), Highly Volatile ($r^{\text{wsd}} \geq 0.0761$).

Alt.	Crit.	$\bar{\mu}$	$\bar{\nu}$	$r^{\max}$	r^{wsd}	Volatility
A_1	e_1	0.7159	0.2125	0.0965	0.0479	Stable
A_1	e_2	0.6570	0.2400	0.0472	0.0414	Stable
A_1	e_3	0.6791	0.2550	0.0355	0.0229	Stable
A_2	e_1	0.5426	0.3585	0.4070	**0.2179**	**Highly Volatile**
A_2	e_2	0.6439	0.2271	0.0821	0.0455	Stable
A_2	e_3	0.6640	0.2166	0.1348	**0.0766**	**Highly Volatile**
A_3	e_1	0.5754	0.2973	0.2461	**0.1188**	**Highly Volatile**
A_3	e_2	0.6211	0.2847	0.1076	**0.0789**	**Highly Volatile**
A_3	e_3	0.5761	0.2930	0.1459	**0.0885**	**Highly Volatile**
A_4	e_1	0.6433	0.2547	0.2690	**0.2134**	**Highly Volatile**
A_4	e_2	0.6158	0.2768	0.1329	**0.1106**	**Highly Volatile**
A_4	e_3	0.5899	0.2723	0.1042	0.0527	Stable
A_5	e_1	0.5878	0.2903	0.2718	**0.1380**	**Highly Volatile**
A_5	e_2	0.5933	0.2713	0.0675	0.0452	Stable
A_5	e_3	0.5426	0.3684	0.2011	**0.1084**	**Highly Volatile**
A_6	e_1	0.6011	0.3144	0.1935	**0.1705**	**Highly Volatile**
A_6	e_2	0.5964	0.3239	0.1163	**0.0970**	**Highly Volatile**
A_6	e_3	0.5952	0.2891	0.0920	0.0645	Slightly Volatile
A_7	e_1	0.6020	0.3052	0.0908	0.0476	Stable
A_7	e_2	0.6000	0.2909	0.0402	0.0351	Stable
A_7	e_3	0.5848	0.3127	0.0777	0.0446	Stable
A_8	e_1	0.4527	0.4208	0.0786	0.0597	Slightly Volatile
A_8	e_2	0.4697	0.3961	0.1237	**0.0918**	**Highly Volatile**
A_8	e_3	0.4876	0.3784	0.0926	0.0583	Slightly Volatile

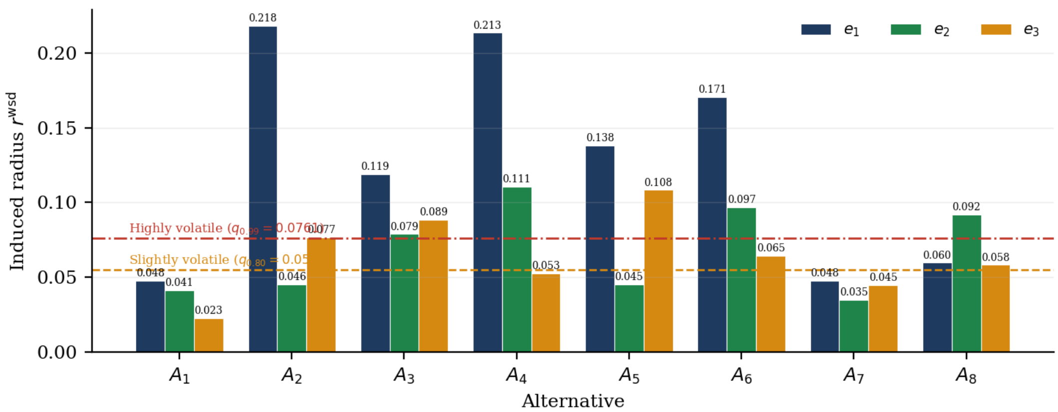

Figure 7. Induced radii r^{wsd} for all $8 \times 3 = 24$ (alternative, criterion) pairs. Dashed/dash-dot lines mark the calibrated band boundaries.

8.3 | Step 3: Criterion Aggregation

Applying the DCIFWA and DCIFWG operators of Section 4 collapses the three per-criterion granules of each alternative into one aggregate CIFV, whose radius carries both the mean and the between-criterion dispersion of the inputs. Table 5 reports the aggregated values under both operators.

Table 5. Aggregated CIFVs per alternative under $\omega = (0.45, 0.35, 0.20)$ and $\lambda = 0.25$. δ is the admissible displacement of Definition 14; here $\delta = \bar{r}/\sqrt{2}$ for every row (the clip is never binding). All outputs satisfy $\bar{\mu} + \bar{\nu} \leq 1$ (Theorem 11).

Alt.	DCIFWA $\langle \bar{\mu}, \bar{\nu}; \bar{r} \rangle$			δ	$\mu - \nu$	DCIFWG $\langle \bar{\mu}, \bar{\nu}; \bar{r} \rangle$		
	$\bar{\mu}$	$\bar{\nu}$	$\bar{r}$			$\bar{\mu}$	$\bar{\nu}$	$\bar{r}$
A_1	0.6891	0.2300	0.0485	0.0343	0.4591	0.6874	0.2308	0.0485
A_2	0.6061	0.2762	0.1510	0.1068	0.3298	0.5998	0.2873	0.1510
A_3	0.5921	0.2920	0.1044	0.0738	0.3001	0.5911	0.2921	0.1044
A_4	0.6235	0.2658	0.1510	0.1068	0.3578	0.6226	0.2660	0.1510
A_5	0.5811	0.2973	0.1097	0.0776	0.2838	0.5804	0.3002	0.1097
A_6	0.5983	0.3124	0.1268	0.0897	0.2859	0.5983	0.3128	0.1268
A_7	0.5979	0.3016	0.0453	0.0320	0.2963	0.5979	0.3018	0.0453
A_8	0.4658	0.4033	0.0760	0.0538	0.0625	0.4655	0.4039	0.0760

8.4 | Step 4: Scoring and Summary

The aggregates are finally scored throughout the spectrum of risk attitude, to show the changes in the ranking of the volatile alternatives as the decision maker transitions from the pessimistic to the optimistic side. The results for the 5 representative attitudes are displayed in Table 6 in terms of scores and induced rankings.

Table 6. Score S_θ (DCIFWA) and ranking as θ varies. The full θ-partition (Section 9) contains 9 regimes separated by 8 exact thresholds; five representative attitudes are shown.

θ	$S(A_1)$	$S(A_2)$	$S(A_3)$	$S(A_4)$	$S(A_5)$	$S(A_6)$	$S(A_7)$	$S(A_8)$	Ranking
0.00	0.4248	0.2230	0.2263	0.2510	0.2062	0.1962	0.2643	0.0087	$A_1 \succ A_7 \succ A_4 \succ A_3 \succ A_2 \succ A_5 \succ A_6 \succ A_8$
0.25	0.4419	0.2764	0.2632	0.3044	0.2450	0.2411	0.2803	0.0356	$A_1 \succ A_4 \succ A_7 \succ A_2 \succ A_3 \succ A_5 \succ A_6 \succ A_8$
0.50	0.4591	0.3298	0.3001	0.3578	0.2838	0.2859	0.2963	0.0625	$A_1 \succ A_4 \succ A_2 \succ A_3 \succ A_7 \succ A_6 \succ A_5 \succ A_8$
0.75	0.4763	0.3832	0.3370	0.4112	0.3226	0.3307	0.3123	0.0894	$A_1 \succ A_4 \succ A_2 \succ A_3 \succ A_6 \succ A_5 \succ A_7 \succ A_8$
1.00	0.4934	0.4366	0.3740	0.4646	0.3613	0.3756	0.3284	0.1162	$A_1 \succ A_4 \succ A_2 \succ A_6 \succ A_3 \succ A_5 \succ A_7 \succ A_8$

Figure 8 shows the DCIFSS data cube and a colour-coded score heat-table across all eight alternatives and five θ values.

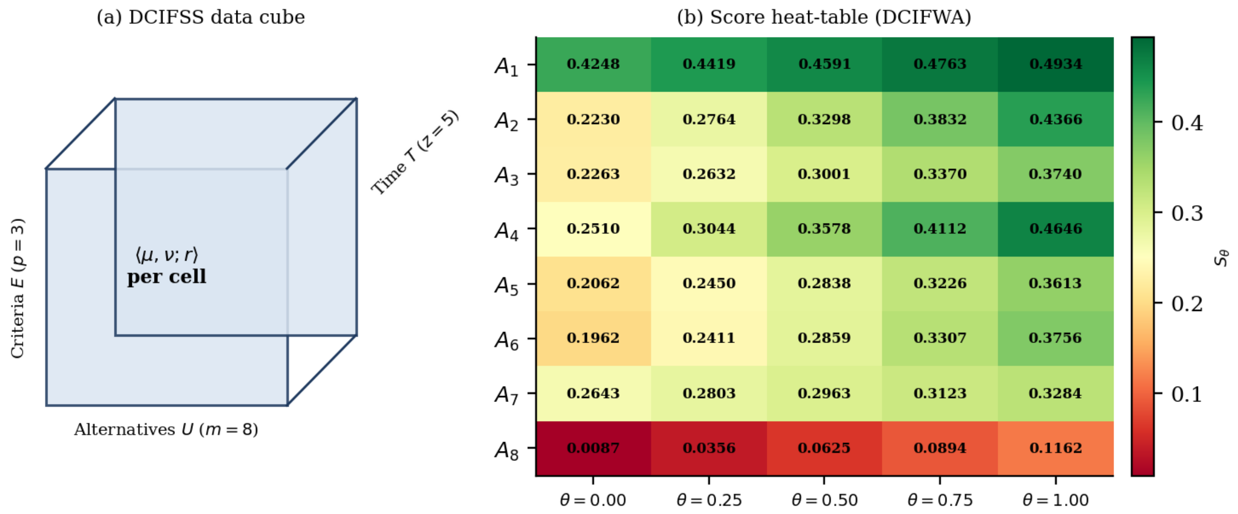

Figure 8. (a) DCIFSS data cube: each cell of the $T \times E \times U$ grid stores a CIFV. **(b)** Colour-coded score heat-table (DCIFWA). A_1 dominates every column; the volatile alternatives (A_2, A_4, A_6) climb as θ increases, reflecting their larger displacement δ.

9 | Sensitivity Analysis

The ranking is only as reliable as it is consistent across the different inputs selected by the analyst; therefore, we show how it changes with the risk attitude and with both weight vectors, where applicable at exact thresholds and where not through Monte Carlo sweeps.

9.1 | Sensitivity to Risk Attitude θ

Because S_θ is affine in θ, the reversal thresholds are the roots of the pairwise score differences and are computed exactly. The 9 resulting regimes partition $[0, 1]$:

θ range	Ranking (DCIFWA)
$[0.0000,\ 0.0499)$	$A_1 \succ A_7 \succ A_4 \succ A_3 \succ A_2 \succ A_5 \succ A_6 \succ A_8$
$[0.0499,\ 0.0889)$	$A_1 \succ A_7 \succ A_4 \succ A_2 \succ A_3 \succ A_5 \succ A_6 \succ A_8$
$[0.0889,\ 0.2760)$	$A_1 \succ A_4 \succ A_7 \succ A_2 \succ A_3 \succ A_5 \succ A_6 \succ A_8$
$[0.2760,\ 0.4121)$	$A_1 \succ A_4 \succ A_2 \succ A_7 \succ A_3 \succ A_5 \succ A_6 \succ A_8$
$[0.4121,\ 0.4544)$	$A_1 \succ A_4 \succ A_2 \succ A_7 \succ A_3 \succ A_6 \succ A_5 \succ A_8$
$[0.4544,\ 0.5905)$	$A_1 \succ A_4 \succ A_2 \succ A_3 \succ A_7 \succ A_6 \succ A_5 \succ A_8$
$[0.5905,\ 0.6379)$	$A_1 \succ A_4 \succ A_2 \succ A_3 \succ A_6 \succ A_7 \succ A_5 \succ A_8$
$[0.6379,\ 0.9492)$	$A_1 \succ A_4 \succ A_2 \succ A_3 \succ A_6 \succ A_5 \succ A_7 \succ A_8$
$[0.9492,\ 1]$	$A_1 \succ A_4 \succ A_2 \succ A_6 \succ A_3 \succ A_5 \succ A_7 \succ A_8$

A_1 leads and A_8 trails throughout $[0, 1]$; all crossings involve the volatile middle group $\{A_2, A_3, A_4, A_5, A_6\}$, whose ordering is precisely what a radius-free model cannot resolve. Figure 9 plots the score lines and marks every threshold.

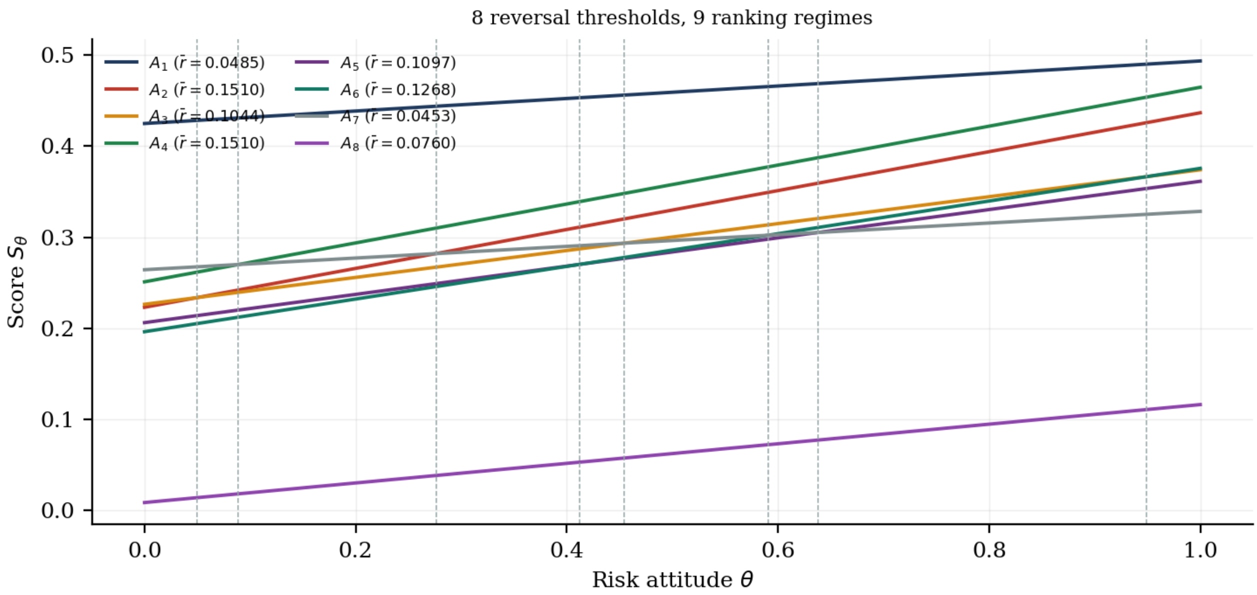

Figure 9. Score S_θ vs. risk attitude θ (DCIFWA). Each line's slope equals $2\delta(\gamma(u))$; the steepest belong to the high-radius alternatives. Dashed verticals mark the exact reversal thresholds.

9.2 | Sensitivity to the Weight Vectors

Table 7 reports three fixed period-weight schemes for the volatile alternatives. The ordering does move with the weights (e.g. A_2 rises from 3rd under recency to 1st under declining weights), which is the expected behaviour of a recency-sensitive method and is quantified here rather than left implicit.

Table 7. Sensitivity of $\bar{r}$ and neutral-attitude score $\mu - \nu$ to the period-weight vector, with the induced $\theta = 0.5$ rank, for the volatile alternatives.

Alt.	Weight scheme	$\bar{\mu}$	$\bar{r}$	$\mu - \nu$	Rank ($\theta = 0.5$)
A_2	Recency	0.6061	0.1510	0.3298	3rd
A_2	Uniform	0.6417	0.1536	0.3907	2nd
A_2	Declining	0.6785	0.1401	0.4539	1st
A_3	Recency	0.5921	0.1044	0.3001	4th
A_3	Uniform	0.5646	0.1124	0.2563	7th
A_3	Declining	0.5372	0.1096	0.2127	7th
A_4	Recency	0.6235	0.1510	0.3578	2nd
A_4	Uniform	0.6228	0.1539	0.3560	3rd
A_4	Declining	0.6221	0.1560	0.3544	4th
A_5	Recency	0.5811	0.1097	0.2838	7th
A_5	Uniform	0.5786	0.1086	0.2765	6th
A_5	Declining	0.5761	0.1069	0.2692	6th
A_6	Recency	0.5983	0.1268	0.2859	6th
A_6	Uniform	0.6238	0.1253	0.3331	4th
A_6	Declining	0.6495	0.1159	0.3810	3rd

To go beyond three hand-picked vectors we sweep both simplices with 10,000 Dirichlet($\mathbf{1}$) draws each (Figure 10). Under period-weight uncertainty A_1 is top-ranked with probability 0.69 and A_2 with probability 0.23 at $\theta = 0.5$, the rest of the mass concentrating on the neighbouring A_4, A_6; under criterion-weight uncertainty A_1's top-rank probability rises to 0.92. The full rank distributions are shown as a heat-map.

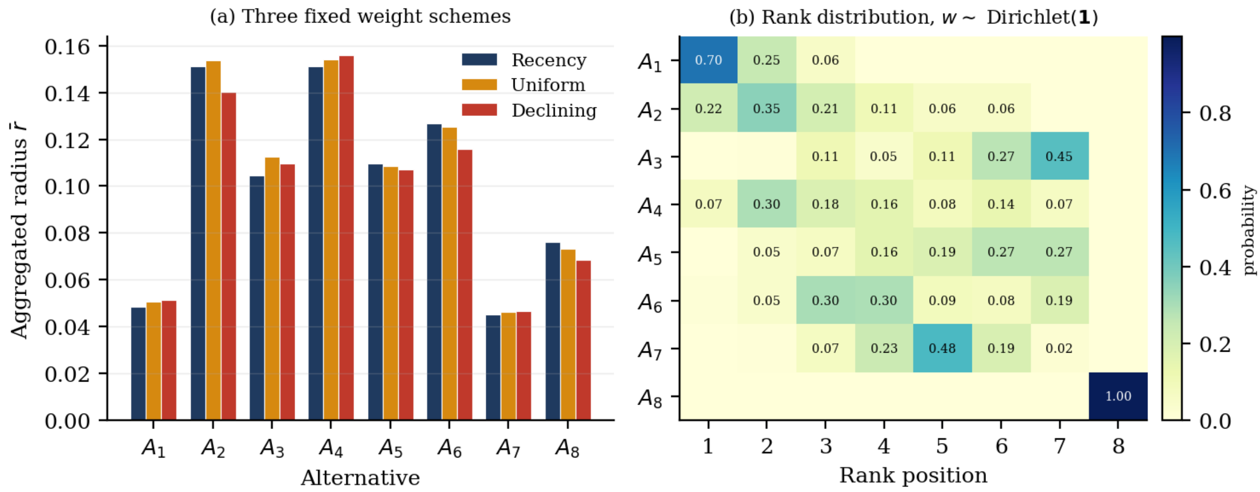

Figure 10. (a) Aggregated radii $\bar{r}$ under three fixed weight schemes. **(b)** Rank-position distribution over 10,000 Dirichlet($\mathbf{1}$) period-weight draws ($\theta = 0.5$); each row sums to one.

10 | Comparative Analysis and Predictive Validation

This section places the DCIFSS beside radius-free baselines and, more importantly, moves past mere difference in rankings to a held-out predictive test that asks whether the volatility-aware score actually forecasts future performance better.

10.1 | Ranking comparison

We compare the DCIFSS against (i) static IFSS (last period, $r \equiv 0$), (ii) dynamic IFSS (time-mean, $r \equiv 0$), and (iii) C-IFS TOPSIS [8] applied to the induced centres. Table 8 lists the rankings and Figure 11 shows the bump chart. As a reduction check, the dynamic-IFSS ordering is reproduced exactly by DCIFSS at , $\theta = \frac{1}{2}$and the risk-free baselines differ only by the score $\mu - \nu$ they employ, not in any way from DCIFSS; we claim nothing about any coincidence being a theorem.

Table 8. DCIFSS vs. radius-free baselines and C-IFS TOPSIS. "Volatility?" records whether the method retains a second-order term after aggregation.

Model	Score	Volatility?	Ranking
Static IFSS (last period)	$\mu-\nu$	No	$A_4 \succ A_1 \succ A_3 \succ A_5 \succ A_7 \succ A_2 \succ A_6 \succ A_8$
Dynamic IFSS (time-mean)	$\mu-\nu$	No	$A_1 \succ A_4 \succ A_2 \succ A_3 \succ A_7 \succ A_6 \succ A_5 \succ A_8$
C-IFS TOPSIS (induced centres)	CC	No	$A_1 \succ A_4 \succ A_7 \succ A_3 \succ A_2 \succ A_6 \succ A_5 \succ A_8$
DCIFSS, $\theta \in [0.000, 0.050)$	S_θ	**Yes**	$A_1 \succ A_7 \succ A_4 \succ A_3 \succ A_2 \succ A_5 \succ A_6 \succ A_8$
DCIFSS, $\theta \in [0.050, 0.089)$	S_θ	**Yes**	$A_1 \succ A_7 \succ A_4 \succ A_2 \succ A_3 \succ A_5 \succ A_6 \succ A_8$
DCIFSS, $\theta \in [0.089, 0.276)$	S_θ	**Yes**	$A_1 \succ A_4 \succ A_7 \succ A_2 \succ A_3 \succ A_5 \succ A_6 \succ A_8$
DCIFSS, $\theta \in [0.276, 0.412)$	S_θ	**Yes**	$A_1 \succ A_4 \succ A_2 \succ A_7 \succ A_3 \succ A_5 \succ A_6 \succ A_8$
DCIFSS, $\theta \in [0.412, 0.454)$	S_θ	**Yes**	$A_1 \succ A_4 \succ A_2 \succ A_7 \succ A_3 \succ A_6 \succ A_5 \succ A_8$
DCIFSS, $\theta \in [0.454, 0.591)$	S_θ	**Yes**	$A_1 \succ A_4 \succ A_2 \succ A_3 \succ A_7 \succ A_6 \succ A_5 \succ A_8$
DCIFSS, $\theta \in [0.591, 0.638)$	S_θ	**Yes**	$A_1 \succ A_4 \succ A_2 \succ A_3 \succ A_6 \succ A_7 \succ A_5 \succ A_8$
DCIFSS, $\theta \in [0.638, 0.949)$	S_θ	**Yes**	$A_1 \succ A_4 \succ A_2 \succ A_3 \succ A_6 \succ A_5 \succ A_7 \succ A_8$
DCIFSS, $\theta \in [0.949, 1]$	S_θ	**Yes**	$A_1 \succ A_4 \succ A_2 \succ A_6 \succ A_3 \succ A_5 \succ A_7 \succ A_8$

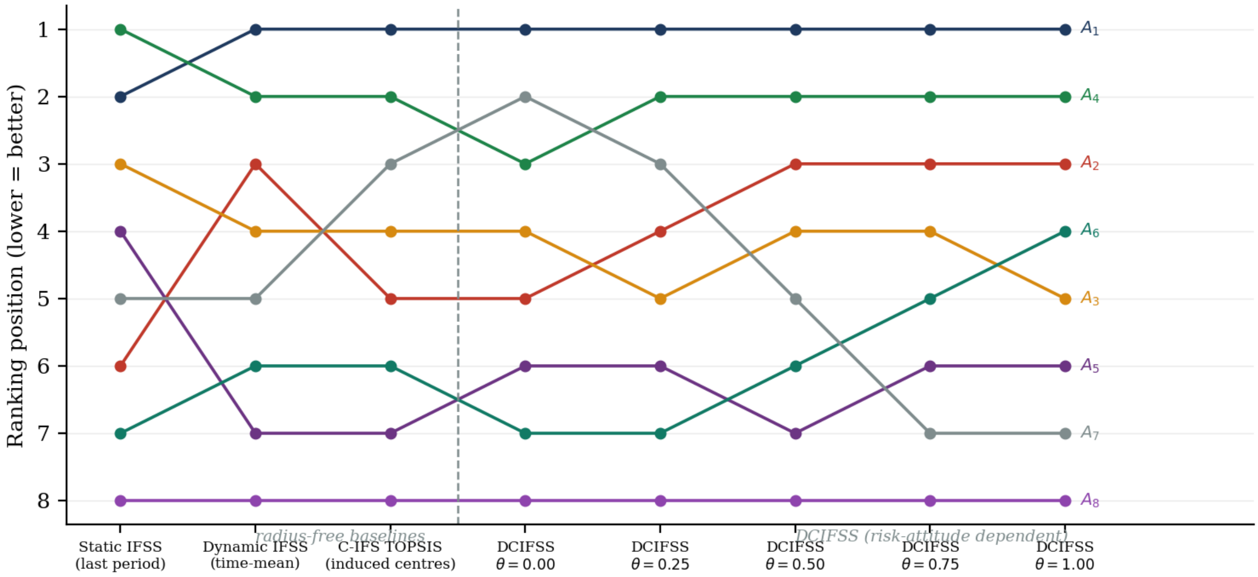

Figure 11. Comparative ranking bump chart. Left of the divider: radius-free baselines (one fixed ranking each). Right: DCIFSS at five θ values. A_1 and A_8 are invariant; crossings among the volatile middle group are visible only in the DCIFSS columns.

A closure stress test over 500,000 i.i.d. CIFV draws (each μ, ν sampled uniformly on the IFIT, r uniform on $[0, \sqrt{2}]$, weights uniform on the simplex) produced zero constraint violations, consistent with Theorem 11.

10.2 | Predictive validation

The decisive question is not whether the DCIFSS ranks differently but whether it ranks better. We answer it with a held-out design. For each of three regimes trend-dominated, mixed, and noise-dominated, differing only in how a fixed total series variance is split between a linear trend and i.i.d. noise we draw 500 scenarios of 8 alternatives over $z + 1 = 6$ periods, rank the alternatives from the first five periods by each method, and score each ranking by its Spearman correlation with the ground-truth ordering at the held-out sixth period. Table 9 reports the mean ρ with 95% confidence intervals.

Table 9. Predictive validation: Spearman ρ between each method's period-1–5 ranking and the realised ordering at the held-out period t_6, over 500 scenarios per regime ($\pm$ 95% CI). Best in each column in **bold**.

Method	Trend-dominated	Mixed	Noise-dominated
Static IFSS (last period)	0.920 ± 0.008	0.806 ± 0.015	0.575 ± 0.023
Dynamic IFSS (time-mean)	0.869 ± 0.010	0.784 ± 0.015	0.612 ± 0.023
C-IFS TOPSIS	0.837 ± 0.013	0.751 ± 0.018	0.579 ± 0.023
DCIFSS θ=0.00	0.851 ± 0.011	0.772 ± 0.016	0.611 ± 0.022
DCIFSS θ=0.25	0.862 ± 0.010	0.780 ± 0.016	0.610 ± 0.022
DCIFSS θ=0.50	0.869 ± 0.010	0.784 ± 0.015	0.612 ± 0.023
DCIFSS θ=0.75	0.872 ± 0.010	0.785 ± 0.015	0.607 ± 0.024
DCIFSS θ=1.00	0.873 ± 0.010	0.781 ± 0.016	0.602 ± 0.025
TA-DCIFSS φ=0.25, $\theta = 0.5$	0.893 ± 0.009	0.803 ± 0.014	0.623 ± 0.023
TA-DCIFSS φ=0.5, $\theta = 0.5$	0.906 ± 0.008	0.812 ± 0.014	0.625 ± 0.022
TA-DCIFSS φ=0.75, $\theta = 0.5$	0.908 ± 0.008	0.811 ± 0.014	0.620 ± 0.022
TA-DCIFSS φ=1, $\theta = 0.5$	0.842 ± 0.013	0.776 ± 0.016	0.606 ± 0.023

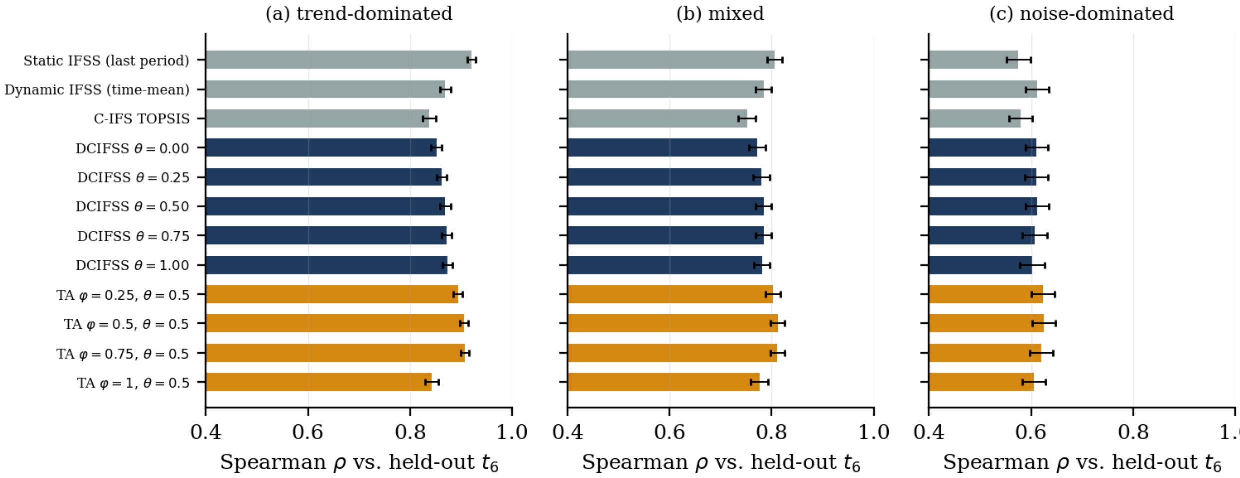

Figure 12. Predictive accuracy (Spearman ρ vs. held-out t_6) by regime. Grey: radius-free baselines; blue: DCIFSS at varying θ; amber: trend-adjusted TA-DCIFSS. The volatility-aware and trend-adjusted models help exactly where their design predicts.

Figure 12 shows the results, which cut both ways. On trend-dominated series the plain last-period baseline is the one to beat, and we do not beat it ($\rho = 0.920$ versus 0.869 for DCIFSS): when quality drifts predictably, the latest reading already carries most of the signal, and docking an alternative for volatility just adds noise. On noise-dominated series the ordering flips. Now the last period is an unreliable draw, so averaging it with a volatility discount helps, and DCIFSS climbs from $\rho = 0.575$ to 0.612. TA-DCIFSS holds up best overall. It takes the mixed regime ($\rho = 0.812$) and stays within a whisker of the last-period baseline even on clean trends ($\rho = 0.906$), since it carries the fitted trend forward and only charges for what is left over once the trend is removed. That residual-versus-trend split is the whole reason Section 6 exists, which is why RQ3 comes out as a quantified "when" and not a flat "yes".

11 | When to Use the Framework

No single variant fits every case, so it is worth being explicit about which one to reach for.

The plain DCIFSS earns its place when the series are noisy and roughly stationary and the decision maker's risk attitude is a real input rather than a nuisance parameter: there the induced radius carries predictive weight, and the θ-partition shows how the ranking swings as that attitude changes. TA-DCIFSS is the better choice when trends are present and their direction matters, so that drift and erraticism are scored apart from one another. And when the trajectory is very short ($z = 2$, where r^{wsd} and $r^{\max}$ collapse onto each other), or so clearly trend-dominated that noise barely registers, a plain last-period or time-mean rule does the job with less overhead. All of this assumes regular sampling and a single expert; irregular spacing, missing periods, regime changes, and multiple assessors fall outside the framework, as the limitations below spell out.

12 | Limitations

We list the main assumptions and boundaries of the study, each of which points to a concrete next step.

L1. Synthetic data only. No real longitudinal dataset is used; real-data validation is the first priority for future work.

L2. Radius choice. r^{wsd} is the weight-consistent primary rule; $r^{\max}$ is kept only as a (weight-inconsistent) robustness variant.

L3. Total dispersion is not uncertainty. Even r^{wsd} conflates trend with noise; TA-DCIFSS (Section 6) separates them but costs an extra parameter φ.

L4. Single expert. Multi-expert aggregation is not formalised.

L5. Weight elicitation. We give no principled method for choosing w, ω, λ, or φ; the Monte Carlo sweep measures how much they matter but does not pick them.

L6. No distance or entropy measures. Full TOPSIS/VIKOR/ELECTRE extensions need distance measures for DCIFVs, which we do not define.

L7. Regular sampling assumed. Irregular spacing and missing periods are not modelled, and the radius's limiting behaviour as $z \to 2$ and $z \to \infty$ is touched on only briefly.

L8. Computational complexity. The $O(mpz)$ cube is tractable at moderate scales; parallelisation is not addressed.

13 | Conclusion

We end by drawing the contributions together, answering the three research questions against the evidence, and pointing to where the framework can go next.

The DCIFSS carries parameterisation, second-order uncertainty, and time at once, and ties them together through a temporally induced radius that is provably admissible under a sharp, data-adaptive bound (Proposition 6) and stable when the period weights are perturbed (Proposition 8). Its risk-attitude score is the Hurwicz criterion adapted to CIFVs, characterised axiomatically (Proposition 17) and made admissible by clipping (Proposition 15). The trend-adjusted variant tells predictable drift apart from genuine erraticism.

RQ1. The radius comes out of the temporal dispersion instead of being supplied by hand, which removes the elicitation burden every prior C-IFS model carries; using the weighted standard deviation keeps it consistent with the period weights.

RQ2. The induced radius obeys the sharp, data-adaptive bound $r^{\mathrm{wsd}} \leq D/\sqrt{2} \leq 1$; for the benchmark's most volatile entry it reaches only 0.6858 of the constant-$\sqrt{2}$ envelope.

RQ3. The predictive test gives a conditional answer rather than a definitional one: the volatility-aware score predicts ranks better on noise-dominated series, the trend-adjusted variant is the most robust across regimes, and the last-period baseline stays ahead on clean trends.

The DCIFWA and DCIFWG operators are closed, idempotent, bounded, and monotone; the Hurwicz score makes the sensitivity analysis exact; and the comparison rests on a held-out predictive test rather than on a claim that the rankings merely differ.

Future directions. Distance and entropy measures for DCIFVs would open the way to TOPSIS and VIKOR extensions [8,9]; the weights $w, \omega, \lambda, \varphi$ need a principled elicitation route, for instance entropy-based period weights [22,26]; and the framework still has to be taken to multi-expert and irregularly-sampled settings and tested on real data in areas such as environmental monitoring, epidemic surveillance, or renewable-energy planning.

Acknowledgements: The authors thank the Department of Mathematics, University of Management and Technology, Lahore, Pakistan, for providing a supportive research environment.

Author Contributions: Conceptualization, M.S.; Methodology, M.S.; Validation, M.S., F.R. and D.Z.M.; Formal Analysis, M.S.; Investigation, M.S.; Writing – Original Draft Preparation, M.S.; Writing – Review & Editing, M.S., F.R. and D.Z.M.; Visualization, M.S.; Supervision, F.R. and D.Z.M. All authors have read and agreed to the published version of the manuscript.

Declaration of Conflicting Interest: The author(s) declared no potential conflicts of interest with respect to the research, authorship, and/or publication of this article.

Funding: The author(s) received no financial support for the research, authorship, and/or publication of this article.

Data Availability Statement: The synthetic numerical examples presented in this study are available on request from the corresponding author.

Plagiarism Statement: This manuscript was screened for textual similarity using Turnitin. The similarity results were found to be within the plagiarism thresholds prescribed by the Higher Education Commission (HEC) of Pakistan and the journal's editorial policy.

Artificial Intelligence (AI) Statement: The authors declare that no generative artificial intelligence tools or

AI-assisted technologies were used in the preparation of this manuscript.

References

[1] L. A. Zadeh, Fuzzy sets, *Information and Control,* 8(1965) 338–353. doi: 10.1016/S0019-9958(65)90241-X.

[2] K. T. Atanassov, Intuitionistic fuzzy sets, *Fuzzy Sets and Systems,* 20(1986) 87–96. doi: 10.1016/S0165-0114(86)80034-3.

[3] D. Molodtsov, Soft set theory—first results, *Computers & Mathematics with Applications,* 37(1999) 19–31. doi: 10.1016/S0898-1221(99)00056-5.

[4] P. K. Maji, R. Biswas, A. R. Roy, Intuitionistic fuzzy soft sets, *Journal of Fuzzy Mathematics,* 9(2001) 677–692.

[5] M. Saeed, M. Hussain, A. A. Mughal, A study of soft sets with soft members and soft elements: A new approach, *Punjab University Journal of Mathematics,* 52(2020) 1–15. ISSN 1016-2526.

[6] K. T. Atanassov, Circular intuitionistic fuzzy sets, *Journal of Intelligent & Fuzzy Systems,* 39(2020) 5981–5986. doi: 10.3233/JIFS-189072.

[7] K. T. Atanassov, E. Marinov, Four distances for circular intuitionistic fuzzy sets, *Mathematics,* 9(2021) 1121. doi: 10.3390/math9101121.

[8] N. Alkan, C. Kahraman, Circular intuitionistic fuzzy TOPSIS method: pandemic hospital location selection, *Journal of Intelligent & Fuzzy Systems,* 42(2022) 295–316. doi: 10.3233/JIFS-219193.

[9] T. Y. Chen, Evolved distance measures for circular intuitionistic fuzzy sets and their exploitation in the technique for order preference by similarity to ideal solutions, *Artificial Intelligence Review,* 56(2023) 7347–7401. doi: 10.1007/s10462-022-10318-x.

[10] I. Otay, S. Çevik Onar, B. Öztayşi, C. Kahraman, A novel interval valued circular intuitionistic fuzzy AHP methodology: Application in digital transformation project selection, *Information Sciences,* 647(2023) 119407. doi: 10.1016/j.ins.2023.119407.

[11] D. Pratama, B. Yusoff, L. Abdullah, A. Kilicman, The generalized circular intuitionistic fuzzy set and its operations, *AIMS Mathematics,* 8(2023) 26758–26781. doi: 10.3934/math.20231370.

[12] A. Unni, S. J. John, T. Baiju, Circular intuitionistic fuzzy soft set theoretic approach to decision making problems, *IEEE Access,* 12(2024) 144818–144836. doi: 10.1109/ACCESS.2024.3472215.

[13] M. Saeed, M. Ahsan, M. H. Saeed, A. U. Rahman, A. Mehmood, M. A. Mohammed, M. M. Jaber, R. Damasevicius, An optimized decision support model for COVID-19 diagnostics based on complex fuzzy hypersoft mapping, *Mathematics,* 10(2022) 2472. doi: 10.3390/math10142472.

[14] M. Arshad, M. Saeed, A. U. Rahman, M. A. Mohammed, K. H. Abdulkareem, J. Nedoma, R. Martinek, M. Deveci, A robust framework for the selection of optimal COVID-19 mask based on aggregations of interval-valued multi-fuzzy hypersoft sets, *Expert Systems with Applications,* 238(2024) 121410. doi: 10.1016/j.eswa.2023.121410.

[15] Z. Xu, Intuitionistic fuzzy aggregation operators, *IEEE Transactions on Fuzzy Systems,* 15(2007) 1179–1187. doi: 10.1109/TFUZZ.2006.890678.

[16] Z. Xu, R. R. Yager, Some geometric aggregation operators based on intuitionistic fuzzy sets, *International Journal of General Systems,* 35(2006) 417–433. doi: 10.1080/03081070600574353.

[17] G. W. Wei, Some geometric aggregation functions and their application to dynamic multiple attribute decision making in the intuitionistic fuzzy setting, *International Journal of Uncertainty, Fuzziness and Knowledge-Based Systems,* 17(2009) 179–196. doi: 10.1142/S0218488509005802.

[18] P. Liu, Y. Wang, Interval-valued intuitionistic fuzzy power average operators and their application to multiple attribute group decision making, *International Journal of Uncertainty, Fuzziness and Knowledge-Based Systems,* 22(2014) 397–420. doi: 10.1142/S0218488514500196.

[19] S. P. Wan, J. Y. Dong, A possibility degree method for interval-valued intuitionistic fuzzy multi-attribute group decision making, *Journal of Computer and System Sciences,* 80(2014) 237–256. doi: 10.1016/j.jcss.2013.07.007.

[20] H. Garg, Generalized intuitionistic fuzzy interactive geometric interaction operators using Einstein t-norm and t-conorm and their application to decision making, *Computers & Industrial Engineering,* 101(2016) 53–69. doi: 10.1016/j.cie.2016.08.017.

[21] Z. Zhang, S. M. Chen, Group decision making with incomplete intuitionistic multiplicative preference relations, *Information Sciences,* 516(2020) 560–571. doi: 10.1016/j.ins.2019.12.042.

[22] D. Rani, H. Garg, Complex intuitionistic fuzzy power aggregation operators and their applications in multi-criteria decision-making, *Expert Systems,* 35(2018) e12325. doi: 10.1111/exsy.12325.

[23] X. Peng, L. Liu, Information measures for q-rung orthopair fuzzy sets, *International Journal of Intelligent Systems,* 34(2019) 1795–1834. doi: 10.1002/int.22115.

[24] L. Hurwicz, Optimality criteria for decision making under ignorance, *Cowles Commission Discussion Paper: Statistics,* No. 370 (1951).

[25] M. Saeed, An introduction to dynamic soft sets: A framework for modeling temporal uncertainty, *Punjab University Journal of Mathematics,* 57(2026) 1131–1163. doi: 10.52280/pujm.2025.57(10)05

[26] M. Saeed, F. Razaq, M. Hassan, M. S. Habib, M. Ullah, Modeling temporal uncertainty using Dynamic Fuzzy Soft Sets: A framework for longitudinal decision-making with time-varying criteria, *Systems and Soft Computing,* 8(2026) 200504.

[27] S. Saleem, M. Riaz, F. Razaq, M. Saeed, Dynamic intuitionistic fuzzy soft set-based WASPAS model for multi-criteria decision making in renewable energy selection, *Argumentation Based Systems Journal,* 2(2026) 208–235. doi: 10.59543/mxct6309

[28] World Health Organization, *Guidelines for Drinking-Water Quality,* 4th ed., WHO, Geneva, 2017. ISBN 978-92-4-154995-0.

[29] P. K. Maji, R. Biswas, A. R. Roy, Fuzzy soft sets, *Journal of Fuzzy Mathematics,* 9(2001) 589–602.